Observation of Density-Dependent Gauge Fields in a Bose-Einstein Condensate Based on Micromotion Control in a Shaken Two-Dimensional Lattice

Logan W. Clark,[1,2,*] Brandon M. Anderson,[1] Lei Feng,[1,2] Anita Gaj,[1,2] K. Levin,[1] and Cheng Chin[1,2]
[1]James Franck Institute, University of Chicago, Chicago, Illinois 60637, USA
[2]Enrico Fermi Institute, University of Chicago, Chicago, Illinois 60637, USA

(Received 13 February 2018; revised manuscript received 27 May 2018; published 18 July 2018)

We demonstrate a density-dependent gauge field, induced by atomic interactions, for quantum gases. The gauge field results from the synchronous coupling between the interactions and micromotion of the atoms in a modulated two-dimensional optical lattice. As a first step, we show that a coherent shaking of the lattice in two directions can couple the momentum and interactions of atoms and break the fourfold symmetry of the lattice. We then create a full interaction-induced gauge field by modulating the interaction strength in synchrony with the lattice shaking. When a condensate is loaded into this shaken lattice, the gauge field acts to preferentially prepare the system in different quasimomentum ground states depending on the modulation phase. We envision that these interaction-induced fields, created by fine control of micromotion, will provide a stepping stone to model new quantum phenomena within and beyond condensed matter physics.

DOI: 10.1103/PhysRevLett.121.030402

Synthesizing gauge fields for cold atoms opens the door to investigate novel quantum phenomena associated with charged particles in an electromagnetic field [1,2]; examples include quantum Hall effects, topological matter, and anyonic excitations. Many experimental approaches have been developed in the past years to introduce gauge fields, including rapidly rotating gases [3–5], Raman transitions [6,7], laser-assisted tunneling [8,9], and lattice shaking [10,11].

As charged particles in motion also generate electromagnetic fields, a complete simulation of the particle-field system should include the feedback of the matter to the gauge field [12]. Such a dynamical gauge field would enable simulation of important models in condensed matter [13–15] and in high energy physics, as in Yang-Mills theories [16]. Many mechanisms have been proposed for introducing dynamical gauge fields in quantum gases [17–22], opening exciting directions for cold atom research.

On the way to dynamical fields, there is a great deal of interest in generating density-dependent (equivalently, interaction-induced) gauge fields in which the effective field depends on the arrangement of atoms [2]. For example, such a field can be used to study new phase transitions [23,24] and one-dimensional particles with anyonic statistics [23,25–27]. Proposals have suggested generating density-dependent gauge fields using light-matter interactions [28,29], lattice modulation [23,25–27], or interaction strength modulation [24]. Experimental realization, however, remains elusive.

Lattice shaking has recently emerged as a promising experimental tool for generating gauge potentials in cold atom systems [30], enabling exciting developments including topological bands [31–33]. In our recent work, lattice modulation at a frequency near-detuned to an interband transition induces a quantum phase transition in Bose-Einstein condensates, resulting in domain formation [11], roton excitations [34], and critical dynamics that are both universal [35] and coherent [36]. In this lattice shaking scheme, the superfluid remains long lived and the atomic interactions play an important role to establish the ordering of superfluid domains.

In this Letter, we experimentally demonstrate an interaction-induced synthetic gauge potential in a Bose-Einstein condensate. The gauge potential $\mathbf{A}(\rho)$ appears as the substitution,

$$\mathbf{q} \to \mathbf{q} - \mathbf{A}(\rho)/\hbar \tag{1}$$

in the Hamiltonian, linking its dependence on the momentum, represented by the wave vector $\mathbf{q} = (q_x, q_y)$, with ρ, the density coarse grained over one unit cell. Equivalently, one can view the interaction-induced field in a tight-binding model as an imaginary part of the tunneling that depends on the occupation number operators $\hat{N}_k$ and $\hat{N}_{k+1}$ of the tunnel coupled sites,

$$J \to J + iJ'(\hat{N}_k + \hat{N}_{k+1}), \tag{2}$$

where J is the tunneling energy without the field and J' encodes the strength of the density-dependent field [37].

To create this density-dependent gauge field we exploit the micromotion of atoms in a shaken 2D square optical

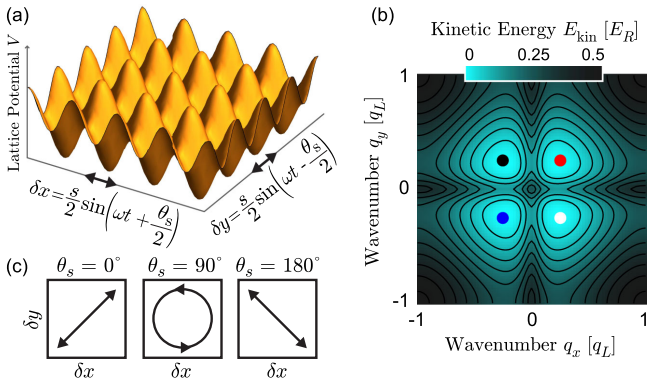

FIG. 1. Atoms in a two-dimensional shaken lattice. (a) A 2D square lattice (orange surface) is shaken by inducing periodic displacements δx and δy along the x and y axes, respectively, (arrows) with equal amplitude s at frequency $\omega \equiv 2\pi/\tau$, shaking period τ, and relative phase θ_s. (b) Shaking above the critical amplitude $s > s_c$ results in a single particle dispersion with four degenerate minima in the ground band at $\mathbf{q} = (+q^*, +q^*)$, $(-q^*, +q^*)$, $(-q^*, -q^*)$, and $(+q^*, -q^*)$, denoted, respectively, by red, black, blue, and white dots. (c) The shaking phase θ_s controls the polarization of the lattice displacement. The polarization does not affect the single particle dispersion shown in (b).

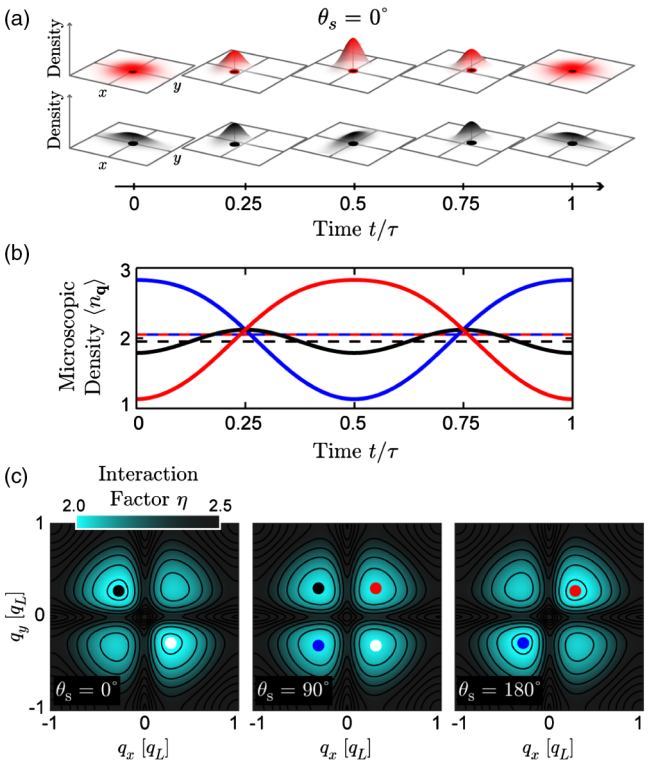

FIG. 2. Interaction-momentum coupling due to micromotion. (a) Examples of micromotion for linear shaking ($\theta_s = 0°$). Snapshots of the density $|\psi_{\mathbf{q}}(x, y, t)|^2$ within a single 2D lattice site are shown for two states, $(+q^*, +q^*)$ (red) and $(-q^*, +q^*)$ (black), within a shaking period τ. (b) As a result of the micromotion, the mean microscopic density $\langle n_{\mathbf{q}}(t) \rangle$ oscillates and reaches a maximum when the wave function is most localized, and a minimum when it is most delocalized. Each curve is colored as in Fig. 1(b); note that the density oscillations of the white state are identical to the plotted black curve. Dashed lines show the averaged densities. (c) Maps of the interaction factor $\eta_{\mathbf{q}}$, equal to the time-averaged microscopic density (see text), for different polarizations. The colored dots mark the ground states after accounting for the interaction factor. Note that circular polarization retains the $D4$ symmetry of the single particle dispersion.

lattice in combination with a periodically modulated interaction strength. For atoms condensed in a two-dimensional momentum state $\mathbf{q}$, this combination yields a mean-field energy shift,

$$\mathcal{E}_{\mathbf{q}} = \eta_{\mathbf{q}} \rho g_0, \tag{3}$$

where $g_0 = \overline{g(t)}$ is the period average of the interaction strength $g(t) = 4\pi\hbar^2 a(t)/m$, $a(t)$ is the scattering length, m is the atomic mass, and $2\pi\hbar$ is Planck's constant. The dimensionless interaction factor $\eta_{\mathbf{q}}$ accounts for the coupling between the micromotion and atomic interactions, as detailed below. A gauge potential in the form of Eq. (1) requires $\eta_{\mathbf{q}}$ to be linear in $\mathbf{q}$.

We perform the experiment in two stages. In the first stage we show the effect of micromotion on interactions by tuning the relative phase θ_s between the lattice shaking in the x and y directions while keeping the scattering length stationary. The micromotion raises the time-averaged interaction energy along the direction of shaking and can break the fourfold symmetry of the dispersion. In the second stage we generate a density-dependent gauge field by modulating the scattering length with a phase θ_g relative to the lattice shaking. This scheme creates a gauge field with $\mathbf{A} \sim \mathbf{e}_\Theta \rho g_0$, where $\mathbf{e}_\Theta$ is a unit vector in the direction $\Theta \equiv \theta_g - \theta_s/2$. In both stages we test for the predicted effects via their influence on the phase transition in the shaken lattice.

Our experiments utilize disk-shaped Bose-Einstein condensates of cesium atoms prepared in a 2D, square optical lattice. The lattice depths along both directions are equal and small enough to maintain superfluidity of the gas. The lattice can then be shaken with identical peak-to-peak amplitudes s and angular frequencies ω along both axes, see Fig. 1(a). The shaking frequency is chosen to be slightly higher than the excitation gap at zero momentum in the lattice [11]. See Supplemental Material for details [37].

When the shaking amplitude s exceeds a critical value s_c, the single particle dispersion $E_{\rm kin}$ develops four minima at momenta $\mathbf{q} = (\pm q^*, \pm q^*)$ and $(\pm q^*, \mp q^*)$, where q^* is controlled by s, see Fig. 1(b). We calculate the effective dispersion of this periodically modulated system using Floquet theory [37]. The fourfold degeneracy is the result of the $D4$ symmetry of the lattice, a 2D generalization of previous experiments in one dimension [11,34–36]. Similar to the 1D system, the change in dispersion induces a phase transition in which the condensate segregates into domains,

each containing atoms occupying one of the four minima. Since the single particle Hamiltonian is separable along the lattice axes, the kinetic energy is independent of the shaking polarization θ_s, defined as the relative phase between the two shaking lattices, see Fig. 1(c).

We first explore the intriguing interplay between micromotion and interactions. Examples of the micromotion, the back-and-forth oscillation of the atomic wave function during one period τ of the lattice shaking, are shown in Fig. 2(a). Since the atomic density depends on the wave function spread in both x and y directions, interactions effectively couple the motion in the two directions and destroy the separability of the system. In particular, the micromotion creates a microscopic density enhancement factor $\langle n_{\mathbf{q}}(t)\rangle = d^2 \int_0^d \int_0^d dx dy |\psi_{\mathbf{q}}(x,y,t)|^4$, where $\psi_{\mathbf{q}}(x,y,t)$ is the (unit-normalized) Floquet steady state wave function and the angle brackets denote the expectation value [37]. The enhancement factor characterizes the ratio of the average density in a lattice site to the coarse-grained density ρ. This enhancement factor oscillates at the shaking frequency and can differ between the four kinetic energy minima, as shown in Fig. 2(b). In this example, the wave function expands and contracts along the x and y axes in phase for momenta along the lattice shaking direction, leading to strong oscillations in density. In contrast, the wave functions along the x and y axes oscillate out of phase for states with momentum perpendicular to the axis of lattice motion, reducing the density oscillation. For circular shaking the wave functions oscillate 90° out of phase for all four momentum states, causing all four to have the same amplitude of density oscillation and therefore the same interaction energy.

Since the typical dynamics of the condensate, including the formation of domains after the phase transition, occur on timescales spanning many shaking periods, they are predominantly sensitive to the interaction energy, $\mathcal{E}_{\mathbf{q}} = \rho \overline{g(t)\langle n_{\mathbf{q}}(t)\rangle}$, where the bar denotes time averaging over one shaking period. Therefore, we define the interaction factor,

$$\eta_{\mathbf{q}} = \frac{1}{g_0} \overline{g(t)\langle n_{\mathbf{q}}(t)\rangle}, \tag{4}$$

which accounts for the interplay between the interaction strength and the micromotion; see Eq. (3).

In the first stage of our experiments, with static interactions $g(t) = g_0$, we control the interaction-momentum coupling by tuning the shaking polarization, as shown in Fig. 2(c). To leading order in q/q_L the interaction factor is

$$\eta_{\mathbf{q}} = \alpha + \beta s^2 \cos\theta_s q_x q_y, \tag{5}$$

where α and β are dimensionless constants that depend on the shaken lattice parameters [37]. The strength of this effect is greatest for linear shaking ($\theta_s = 0°$ or 180°), with which the momentum states along the axis of lattice motion experience much stronger density modulation, leading to a higher interaction factor than the momentum states perpendicular to the axis of lattice motion (hereafter "off-diagonal states"), whose density is more constant over time. This effect causes domains to form preferentially in the off-diagonal states.

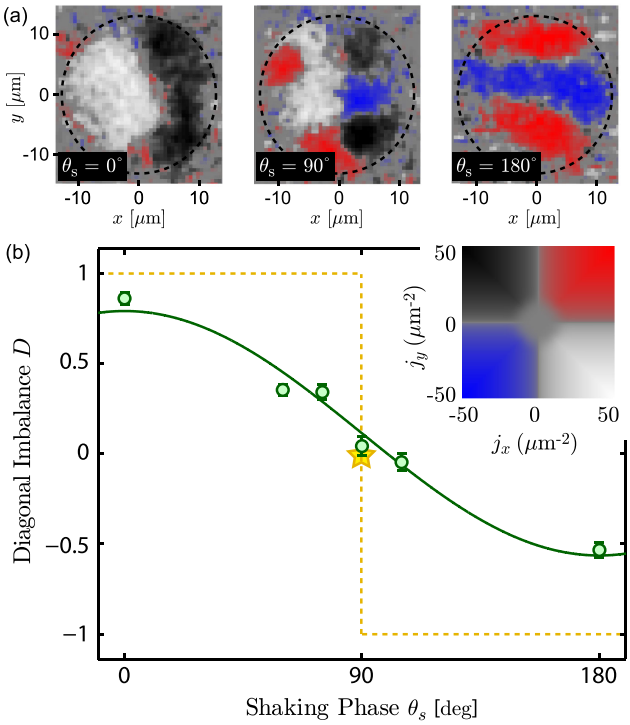

FIG. 3. Observed coupling of interaction and momentum. (a) Example, reconstructed domain structures (see text) representing the density profiles of atoms in each well, measured after crossing the phase transition with the shaking polarizations indicated on each image. The dashed circles guide the eye to the region containing the condensate. The correspondence between color and pseudospin density (see text) is shown in the upper-right corner of panel (b). (b) The imbalance D (see text) of the atomic populations between the two quasimomentum diagonals characterizes the anisotropy which results from the quasimomentum-dependent interactions for different polarizations. The solid curve is a sinusoidal fit. The orange, dashed curve shows the expected imbalance in the absolute ground state; the star emphasizes that the expected imbalance is $D = 0$ for circular shaking ($\theta_s = 90°$).

We test for the presence of interaction-momentum coupling by driving condensates across the phase transition with different shaking phases θ_s and measuring the resulting quasimomentum distribution. After loading the condensate into the lattice, we linearly ramp up the shaking amplitude, exceeding the critical amplitude and thus driving the condensate across the phase transition. After a brief time of flight we measure the density distributions $n_i(\mathbf{r})$ of atoms occupying the quasimomentum state in the ith quadrant; for example, n_1 is the density in the $(+q^*, +q^*)$ state. Finally, we calculate the pseudospin density along

each lattice axis, $j_x = n_1 + n_4 - n_2 - n_3$ and $j_y = n_1 + n_2 - n_3 - n_4$. See Supplemental Material for details [37].

Typical reconstructed domain images for various shaking polarizations are shown in Fig. 3(a). To better quantify the biasing of the domains toward particular wells for ensembles of many images, we introduce an imbalance factor $D = (N_2 + N_4 - N_1 - N_3)/N_{\mathrm{tot}}$, where N_i is the population in the ith quadrant and N_{tot} is the total atom number. We observe a clear, polarization-dependent biasing of the domains toward forming in off-diagonal states, indicative of interaction-momentum coupling, see Fig. 3(b). For linear shaking, which maximizes the interaction-momentum coupling, the diagonal imbalance approaches 1 (−1) with $\theta_s = 0°$ (180°), as expected. Under these conditions, the $D4$ symmetry of the ground states is clearly broken by interactions. As the shaking polarization becomes more circular, the imbalance is progressively reduced. For precisely circular shaking ($\theta_s = 90°$) the interaction-momentum coupling disappears and the $D4$ symmetry is restored, resulting in a diagonal imbalance of $D = 0.04(5)$ consistent with zero. Because of the finite ramp speed in our experiments, the phase transition is not adiabatic [35]. As a result, the bias of the gas toward off-diagonal states increases with the energy difference between the wells. This effect causes the magnitude of the diagonal imbalance to smoothly increase as the interaction-momentum coupling is enhanced by tuning the shaking polarization from circular toward linear, as observed in Fig. 3(b).

In the second stage of our experiments, we generate a density-dependent gauge field by applying synchronized shaking and interaction strength modulation. We tune the magnetic field near a Feshbach resonance [39] to modulate the interaction strength as $g(t) = g_0 - g_1 \cos(\omega t - \theta_g)$ at the same frequency as the lattice shaking and with phase θ_g; see Fig. 4(a). In this case, the interaction-momentum coupling can be understood intuitively by comparing the microscopic density and the interaction strength during each shaking period; see Fig. 4(a). When the interaction strength oscillates in phase (out of phase) with the density, the interaction energy is maximized (minimized).

To quantify the interaction-induced field, the interaction factor can be decomposed as, see Eq. (4),

$$\eta_{\mathbf{q}} = \eta_{\mathbf{q}}^{(0)} + \frac{g_1}{g_0}\eta_{\mathbf{q}}^{(1)}, \tag{6}$$

where $\eta_{\mathbf{q}}^{(0)} = \overline{\langle \eta_{\mathbf{q}}(t) \rangle}$ is the static interaction factor and $\eta_{\mathbf{q}}^{(1)} = -\overline{\langle \eta_{\mathbf{q}}(t) \rangle \cos(\omega t - \theta_g)}$ is the modulated interaction factor. We use circular shaking ($\theta_s = 90°$) so that the static interaction factor maintains the $D4$ symmetry. For small momentum $|\mathbf{q}| \ll q_L$ the modulated interaction factor takes the form [37],

$$\eta_{\mathbf{q}}^{(1)} = -\sqrt{\frac{\alpha\beta}{2}} s \mathbf{e}_\Theta \cdot \mathbf{q}, \tag{7}$$

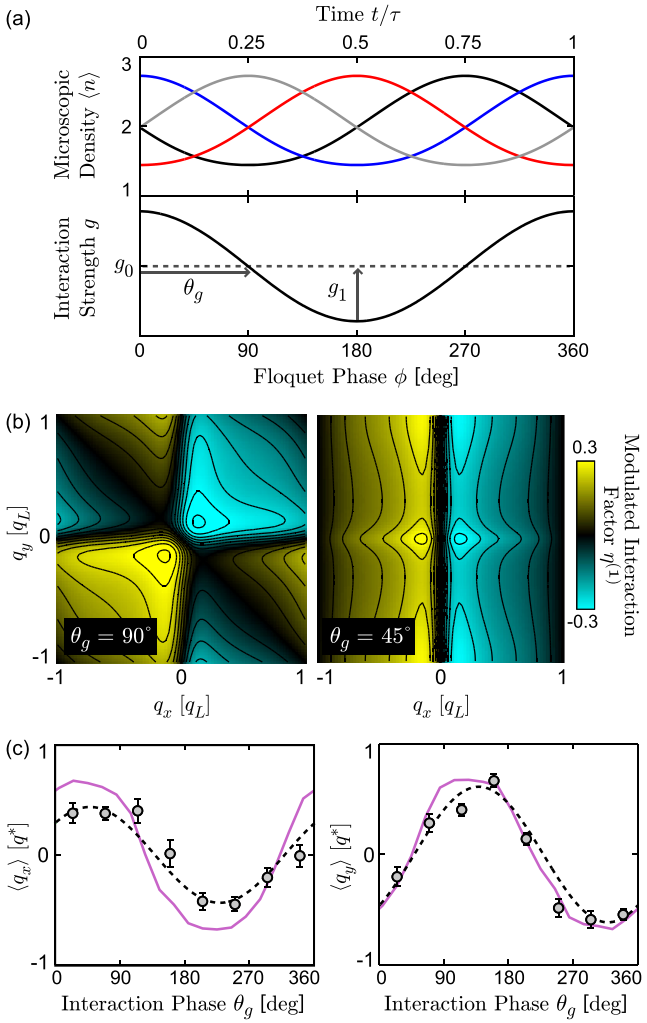

FIG. 4. Density-dependent synthetic field from synchronized shaking and interaction strength modulation. (a) The upper panel plots the mean, microscopic density for circular shaking ($\theta_s = 90°$). Each curve is colored as in Fig. 1(b). The lower panel shows the modulated interaction strength $g(t) = g_0 - g_1 \cos(\omega t - \theta_g)$. The modulated interactions raise (lower) the energy of quasimomentum states whose density oscillates in phase (out of phase) with the interaction modulation. (b) Modulated interaction factors for $\theta_g = 90°$ (left) and $\theta_g = 45°$ (right). (c) Measurement of the average quasimomentum of the condensate ($q^* = 0.08 q_L$) in the presence of the interaction-induced field (circles). Error bars show standard error. The dashed curves show simultaneous, sinusoidal fits, which yield a phase offset of only $4 \pm 3°$ from expectations. Simulations using the Gross-Pitaevskii equation [40] (solid magenta curves) agree well with the experiment.

which corresponds to the density-dependent gauge potential,

$$\mathbf{A}(\rho) = \sqrt{\frac{\alpha\beta}{2}} m s g_1 \rho \mathbf{e}_\Theta, \tag{8}$$

whose direction is given by $\mathbf{e}_\Theta$ with $\Theta \equiv \theta_g - \theta_s/2$. The equivalent treatment of the gauge field in terms of an

occupation-dependent Peierls phase does not rely on the small momentum limit [37]. The static interaction factor $\eta_{\mathbf{q}}^{(0)}$, which does not correspond to a gauge potential, can be made negligible by reducing the average interaction strength g_0. Salient examples of the modulated interaction factors from a numerical calculation are shown in Fig. 4(b).

Experimentally, we test for the interaction-induced gauge field by measuring the bias toward particular quasimomenta as a function of the interaction phase θ_g. We first prepare the condensate in a stationary lattice with an oscillating scattering length. We then begin to circularly shake the lattice, linearly increasing the shaking amplitude and driving the system across the phase transition. After a brief settling time, we measure the momentum distribution $\rho(\mathbf{q})$ based on time-of-flight expansion [36] and calculate the average quasimomentum $\langle \mathbf{q} \rangle = \int \mathbf{dqq}\rho(\mathbf{q})$ [37].

The average quasimomentum after the phase transition shows a clear bias depending on the interaction modulation phase θ_g, indicative of the interaction-induced gauge field, see Fig. 4(c). Based on the form of the gauge potential shown in Eq. (7), we expect the biasing along the x and y axes to take the approximate forms $\langle q_x \rangle \propto \cos(\theta_g - 45°)$ and $\langle q_y \rangle \propto \sin(\theta_g - 45°)$. Simultaneous, sinusoidal fits to the data in Fig. 4(c) yield a phase consistent with this prediction. The magnitude of the bias in momentum does not reach q^*, since it depends sensitively on the dynamics of crossing the phase transition [11,35] as well as the magnitude of the gauge potential. In principle, the size of the interaction induced field, and therefore the bias, can be increased by using a larger interaction modulation amplitude. However, doing so can induce other instabilities in the gas [41–43].

To confirm that the magnitude of the observed effect matches theoretical expectations, we have performed simulations of this experiment using the Gross-Pitaevskii equation [40]. The resulting magenta curves in Fig. 4(c), which show the average outcomes of five simulations at each θ_g (20° steps) with different random noise seeds, agree nicely with our experiments.

In summary, we have demonstrated an interaction-induced gauge field based on synchronous lattice shaking and interaction strength modulation. Our work presents a paradigm to guide the simulation of gauge field theories using ultracold atom systems. For example, this scheme can be used directly to simulate the anyon-Hubbard model [23,25–27], as detailed in the Supplemental Material [37].

L. W. C. was supported by a Grainger Graduate Fellowship. This work was supported by NSF Grant No. PHY-1511696, Army Research Office-Multidisciplinary Research Initiative Grant No. W911NF-14-1-0003, and the University of Chicago Materials Research Science and Engineering Center, which is funded by the National Science Foundation under Grant No. DMR-1420709.

*lwclark@uchicago.edu

[1] J. Dalibard, F. Gerbier, G. Juzeliūnas, and P. Öhberg, Rev. Mod. Phys. **83**, 1523 (2011).
[2] N. Goldman, G. Juzeliūnas, P. Öhberg, and I. B. Spielman, Rep. Prog. Phys. **77**, 126401 (2014).
[3] K. W. Madison, F. Chevy, W. Wohlleben, and J. Dalibard, Phys. Rev. Lett. **84**, 806 (2000).
[4] J. R. Abo-Shaeer, C. Raman, J. M. Vogels, and W. Ketterle, Science **292**, 476 (2001).
[5] V. Schweikhard, I. Coddington, P. Engels, V. P. Mogendorff, and E. A. Cornell, Phys. Rev. Lett. **92**, 040404 (2004).
[6] Y.-J. Lin, R. L. Compton, K. Jimenez-Garcia, J. V. Porto, and I. B. Spielman, Nature (London) **462**, 628 (2009).
[7] Y. J. Lin, K. Jiménez-García, and I. B. Spielman, Nature (London) **471**, 83 (2011).
[8] H. Miyake, G. A. Siviloglou, C. J. Kennedy, W. C. Burton, and W. Ketterle, Phys. Rev. Lett. **111**, 185302 (2013).
[9] M. Aidelsburger, M. Atala, M. Lohse, J. T. Barreiro, B. Paredes, and I. Bloch, Phys. Rev. Lett. **111**, 185301 (2013).
[10] J. Struck, M. Weinberg, C. Ölschläger, P. Windpassinger, J. Simonet, K. Sengstock, R. Höppner, P. Hauke, A. Eckardt, M. Lewenstein, and L. Mathey, Nat. Phys. **9**, 738 (2013).
[11] C. V. Parker, L.-C. Ha, and C. Chin, Nat. Phys. **9**, 769 (2013).
[12] U.-J. Wiese, Ann. Phys. (Berlin) **525**, 777 (2013).
[13] L. Savary and L. Balents, Rep. Prog. Phys. **80**, 016502 (2017).
[14] G. Baskaran and P. W. Anderson, Phys. Rev. B **37**, 580 (1988).
[15] M. Levin and X.-G. Wen, Rev. Mod. Phys. **77**, 871 (2005).
[16] I. J. R. Aitchison and A. J. Hey, *Gauge Theories in Particle Physics: A Practical Introduction* (Institute of Physics Publishing, Bristol and Philadelphia, 1989).
[17] D. Banerjee, M. Dalmonte, M. Müller, E. Rico, P. Stebler, U.-J. Wiese, and P. Zoller, Phys. Rev. Lett. **109**, 175302 (2012).
[18] J. I. Cirac, P. Maraner, and J. K. Pachos, Phys. Rev. Lett. **105**, 190403 (2010).
[19] E. Kapit and E. Mueller, Phys. Rev. A **83**, 033625 (2011).
[20] E. Zohar and B. Reznik, Phys. Rev. Lett. **107**, 275301 (2011).
[21] E. Zohar, J. I. Cirac, and B. Reznik, Phys. Rev. Lett. **110**, 055302 (2013).
[22] L. Tagliacozzo, A. Celi, P. Orland, M. W. Mitchell, and M. Lewenstein, Nat. Commun. **4**, 2615 (2013).
[23] T. Keilmann, S. Lanzmich, I. McCulloch, and M. Roncaglia, Nat. Commun. **2**, 361 (2011).
[24] S. Greschner, G. Sun, D. Poletti, and L. Santos, Phys. Rev. Lett. **113**, 215303 (2014).
[25] S. Greschner and L. Santos, Phys. Rev. Lett. **115**, 053002 (2015).
[26] L. Cardarelli, S. Greschner, and L. Santos, Phys. Rev. A **94**, 023615 (2016).
[27] C. Sträter, S. C. L. Srivastava, and A. Eckardt, Phys. Rev. Lett. **117**, 205303 (2016).
[28] M. J. Edmonds, M. Valiente, G. Juzeliūnas, L. Santos, and P. Öhberg, Phys. Rev. Lett. **110**, 085301 (2013).

[29] M. J. Edmonds, M. Valiente, and P. Ohberg, J. Phys. B **46**, 134013 (2013).
[30] A. Eckardt, Rev. Mod. Phys. **89**, 011004 (2017).
[31] G. Jotzu, M. Messer, R. Desbuquois, M. Lebrat, T. Uehlinger, D. Greif, and T. Esslinger, Nature (London) **515**, 237 (2014).
[32] N. Fläschner, B. S. Rem, M. Tarnowski, D. Vogel, D.-S. Lühmann, K. Sengstock, and C. Weitenberg, Science **352**, 1091 (2016).
[33] M. Tarnowski, F. N. Ünal, N. Fläschner, B. S. Rem, A. Eckardt, K. Sengstock, and C. Weitenberg, arXiv:1709.01046.
[34] L.-C. Ha, L. W. Clark, C. V. Parker, B. M. Anderson, and C. Chin, Phys. Rev. Lett. **114**, 055301 (2015).
[35] L. W. Clark, L. Feng, and C. Chin, Science **354**, 606 (2016).
[36] L. Feng, L. W. Clark, A. Gaj, and C. Chin, Nat. Phys. **14**, 269 (2018).
[37] See Supplemental Material at http://link.aps.org/supplemental/10.1103/PhysRevLett.121.030402 for details, which includes Ref. [38].
[38] W. Zheng, B. Liu, J. Miao, C. Chin, and H. Zhai, Phys. Rev. Lett. **113**, 155303 (2014).
[39] C. Chin, R. Grimm, P. Julienne, and E. Tiesinga, Rev. Mod. Phys. **82**, 1225 (2010).
[40] B. M. Anderson, L. W. Clark, J. Crawford, A. Glatz, I. S. Aranson, P. Scherpelz, L. Feng, C. Chin, and K. Levin, Phys. Rev. Lett. **118**, 220401 (2017).
[41] S. E. Pollack, D. Dries, R. G. Hulet, K. M. F. Magalhães, E. A. L. Henn, E. R. F. Ramos, M. A. Caracanhas, and V. S. Bagnato, Phys. Rev. A **81**, 053627 (2010).
[42] L. W. Clark, A. Gaj, L. Feng, and C. Chin, Nature (London) **551**, 356 (2017).
[43] L. Feng, J. Hu, L. W. Clark, and C. Chin, arXiv:1803.01786.